Applied Catalysis B: Environmental 254 (2019) 76–85

Contents lists available at ScienceDirect

Applied Catalysis B: Environmental

journal homepage: www.elsevier.com/locate/apcatb

Effects of H_2O on HCHO and CO oxidation at room-temperature catalyzed by MCo_2O_4 (M = Mn, Ce and Cu) materials

Chunyan Ma[a,1], Chenggong Yang[a,b,1], Bin Wang[c], Cheng Chen[a], Fengbang Wang[a,b], Xinglei Yao[a], Maoyong Song[a,*]

[a] Key Laboratory of Environmental Nanotechnology and Health Effects, Research Center for Eco-Environmental Sciences, Chinese Academy of Sciences, Beijing, 100085, China
[b] University of Chinese Academy of Sciences, Beijing, 100049, China
[c] Beijing Research Institute of Chemical Industry, Sinopec Group, Beijing, 100013, China

ARTICLE INFO

Keywords:
H_2O effect
Catalytic performance
HCHO oxidation
CO oxidation
Reaction mechanism

ABSTRACT

The abatement of HCHO and CO at room temperature by catalytic oxidation over metal oxides can be achieved. However, the catalytic performance of metal oxides is influenced by H_2O vapor in the reaction air and the mechanism of H_2O role is still debated. In this paper, the effect of H_2O on the catalytic performance of an MCo_2O_4 (M = Mn, Ce and Cu) catalyst for HCHO and CO oxidation at room temperature was investigated. For both HCHO oxidation and CO oxidation, all the MCo_2O_4 catalysts in humid air are less active than in dry air except for HCHO oxidation catalyzed by $CuCo_2O_4$ catalyst. The $CuCo_2O_4$ is inactive for HCHO oxidation in dry air, but active for HCHO oxidation in humid air. XRD and XPS results indicated that there are no obvious changes of crystal structure and valance states of element between fresh and used MCo_2O_4 catalysts. The active sites of MCo_2O_4 catalysts and reaction/deactivation mechanism of HCHO and CO oxidation were studied by H_2O-TPD and DRIFT. The associatively adsorbed H_2O on MCo_2O_4 contributed to the active HOH sites for HCHO oxidation. Formate species are intermediates of HCHO oxidation. However, if formate cannot be further transferred into CO_2, the formate adsorbed on active sites will result in catalyst deactivation. In humid air, hydrogen-bonded OH and free OH generated and covered active sites accelerated the catalyst deactivation in HCHO oxidation. The CO was oxidized by the active oxygen species but not included OH species. Thus, the H_2O adsorbed on oxygen vacancies blocked the generation of active oxygen species, which resulted in MCo_2O_4 deactivation for CO oxidation in humid air. This work provide a fundamental understanding of the key role of H_2O in the HCHO and CO oxidation at room temperature, which is helpful for the design of high activity and long lifetime catalyst used in dry or humid conditions.

1. Introduction

Formaldehyde is one of the major indoor air pollutants emitted from furniture and decorations that is hazardous to human health [1]. Long-term exposure to low concentrations of formaldehyde is possibly carcinogenic to humans [2]. In recent decades, many studies have been performed on the removal of formaldehyde, including physical adsorption [3], photo-catalytic oxidation [4,5], plasma decomposition with a catalyst [6] and catalytic oxidation [7,8]. Among them, room temperature catalytic oxidation is workable for the removal of HCHO, because this method does not require the addition of light sources and heat sources [9]. In addition; CO is a harmful air pollutant in indoor spaces, which can be easily oxidized to CO_2 over catalysts at room temperature [10].

Many catalysts have been found to completely oxidize HCHO and CO to CO_2 and H_2O at room temperature, including supported noble metal catalysts [11–15] and non-noble catalysts [16–19]. Metal oxide catalysts are valuable due to their lower cost compared with supported noble catalysts. The reported reaction mechanism of formaldehyde oxidation over supported noble metal catalysts is different from metal oxide catalysts. It has been pointed out that CO is the key intermediate in the HCHO oxidation over Pt/TiO_2 [11] and Ag/MCM-41 catalysts [12]. Some kinds of formate species were identified as intermediates for HCHO oxidation over MnO_x-CeO_2 [16]], Co_3O_4-CeO_2 [17] and CuO

* Corresponding author.
E-mail address: smsong@rcees.ac.cn (M. Song).
[1] These authors contributed equally.

https://doi.org/10.1016/j.apcatb.2019.04.085
Received 14 February 2019; Received in revised form 22 April 2019; Accepted 23 April 2019
Available online 27 April 2019
0926-3373/ © 2019 Published by Elsevier B.V.

[18]. Dioxymethylene (DOM) was identified as an intermediate for HCHO oxidation over $Mn_xCo_{3-x}O_4$ [20]. Co_3O_4 [21], MnO_2-Co_3O_4-CeO_2 [10]. $Mn_{0.75}Co_{2.25}O_4$ [19] catalysts have been reported to oxidize CO at room temperature. The carbonates and formate species were identified as intermediates of CO oxidation over $Mn_{0.75}Co_{2.25}O_4$ catalysts [19]. It can be seen that formate species are intermediates for HCHO oxidation and CO oxidation, which still have value to be studied further.

As mentioned above, MnO_2, Co_3O_4, CeO_2, CuO and the related mixture oxides may show catalytic activity for HCHO and CO oxidation at room temperature. However, the catalytic activities and stabilities could be influenced by the H_2O vapor in the reaction gas [19,22]. The activities of HCHO oxidation over MnO_x [2], and $Mn_{0.75}Co_{2.25}O_4$ [19] could be enhanced by H_2O vapor in the reaction gas. However, the catalytic activity of HCHO oxidation over MnO_x-CeO_2 decreased with H_2O vapor increased in the reaction gas [22]. For CO oxidation catalyzed by metal oxides (such as Co_3O_4 [21,23–25], and CuO [26–28]), the catalytic activity of the catalysts in humid condition is lower than that in dry condition. The reaction and deactivation mechanisms of HCHO and CO oxidation over metal oxides affected by H_2O are still debated. Zhang et al. [2] reported that the oxidation activity of formaldehyde in humid conditions (relative humidity (RH) = 33% and 65%) is higher than in dry conditions. Thus, they concluded that water vapor is essential to HCHO oxidation. Hydroxyl radical (OH) from water vapor dissociation favors the adsorption and transfer of oxygen on the MnO_x catalysts, which is very important during HCHO oxidation. However, when the relative humidity increased to 92%, the catalytic activity decreased, which was not explained in their article. In addition, Shi et al. [19] reported that the conversion of CO to CO_2 over $Mn_{0.75}Co_{2.25}O_4$ in dry air is higher than that in humid air (RH = 50%), because water blocked the active sites and prevented the adsorption of CO and O_2. However, the catalytic stability of CO oxidation over $Mn_{0.75}Co_{2.25}O_4$ in humid air increased. Thus, the mechanism of the effect of H_2O on HCHO and CO oxidation over metal oxides is still worth to be studied.

Here, we synthesized some cobalt-based complex oxide catalysts including $MnCo_2O_4$, $CeCo_2O_4$ and $CuCo_2O_4$. The effect of H_2O on the activity and stability of both HCHO and CO oxidation over MCo_2O_4 was investigated. The reaction and deactivation mechanisms of HCHO and CO oxidation over MCo_2O_4 catalysts in dry air or in humid air were proposed. The understanding of the reaction and deactivation mechanisms will help us develop catalyst with excellent catalytic performance for HCHO and CO oxidation at room temperature.

2. Experiment

2.1. Preparation of MCo_2O_4

MCo_2O_4 catalysts were synthesized by a sol-gel citric acid method. Taking $MnCo_2O_4$ as an example, 0.01 mol $Mn(NO_3)_2$ was dissolved in 50 mL of ultra-pure water and stirred until they formed a solution. Then, 0.02 mol of $Co(NO_3)_2{\cdot}6H_2O$ was dissolved in this solution under vigorous stirring at 30 °C. Afterward, a corresponding amount of citric acid was added to the obtained solution. The molar ratio of citric acid to total metal ion was kept at 1.2:1. After 30 min of constant stirring, the citric acid was completely dissolved. Then, the above solution was gradually heated to 80 °C and continuously stirred for 4 h at this temperature to form a gel. The resulting gels were dried at 100 °C for 12 h, and then calcined at 350 °C in air for 4 h. The as-synthesized sample was called $MnCo_2O_4$.

The synthetic procedures for $CuCo_2O_4$ and $CeCo_2O_4$ were similar to that of $MnCo_2O_4$ except that $Mn(NO_3)_2$ was replaced by $Cu(NO_3)_2$ and $Ce(NO_3)_2$, respectively.

2.2. Characterization

The Brunauer-Emmett-Teller (BET) specific surface area was measured on Micromeriticis ASAP 2020 analyzer by nitrogen physisorption at 77 K. X-ray diffraction (XRD) patterns were recorded on an X'Pert PRO (PANalytical) diffractometer equipped with a Cu Kα radiation source (λ = 0.15418 nm). A continuous mode was used for collecting data in the 2θ range from 5 to 90° at a scan step of 0.02°. Raman measurements were carried out with a 532 nm laser and a power of 0.6 mW on a HR-Evolution spectrophotometer. H_2-temperature programmed reduction (H_2-TPR) and oxygen temperature programmed desorption (O_2-TPD) were performed in Micromeritics Chemisorb 2720 instrument. Prior to each TPR run, 20 mg sample was placed in a U-type quartz reactor. The catalyst was pretreated in the He flow at 300 °C for 60 min, then it was cooled down to 30 °C in the He flow. The sample was reduced by 2% H_2/He gas flow at 50 mL· min^{-1} from 30 to 900 °C with a heating rate of 10 °C· min^{-1}. The procedures of O_2-TPD were as follows: 50 mg samples were pretreated under a He flow at 300 °C for 60 min, then it was cooled down to 30 °C in the He flow. Flowed the sample was purged with 5% O_2/He gas flow at 50 mL· min^{-1} for 30 min at room temperature, then it was swept by a pure He gas flow at 50 mL· min^{-1} for 30 min. Afterward, the sample was heated to 900 °C with a heating rate of 10 °C· min^{-1} under a pure He gas flow. H_2O temperature-programmed desorption (H_2O-TPD) analyses were performed using a purpose-built TPD apparatus equipped with a mass analyzer. Then, 0.05 g samples were taken and purged with He at 30 °C until the signal was stable, and then heated to 600 °C at 10 °C· min^{-1}. An online analysis system equipped with a mass spectrometer was used to monitor the evolved gas (water, 18 amu). *In-situ* diffuse reflectance infrared Fourier transform (DRIFT) spectroscopy was recorded on a Bruker VERTEX 70 instrument scanning from 3800 to 1200 cm^{-1} at a resolution of 4 cm^{-1}. Before the beginning of DRIFT experiments, the catalysts were swept by N_2 gas for 30 min at 120 °C. Afterwards, the sample cell was allowed to cool to 25 °C. For HCHO oxidation, 355 ppm HCHO/21% O_2/N_2 balance in dry air or in humid air (RH = 45%) at a flow rate of 40 mL· min^{-1} passing through the sample cell. For CO oxidation, 200 ppm CO/21% O_2/N_2 balance in dry air or in humid air (RH = 55%) at a flow rate of 40 mL· min^{-1} passing through the sample cell. DRIFT spectra were recorded until the catalysts deactivated.

2.3. Catalytic oxidation

2.3.1. Formaldehyde oxidation

Catalytic tests were performed using a fixed bed reactor loaded with 0.2 g of catalyst (40–60 mesh). The reaction feed consisted of 355 ppm formaldehyde with the gas mixture (O_2: 21%, He: balance). In this experiment, a boat shape flask containing formaldehyde solution (formalin) was used. 21% O_2/He balance gas flow the boat shape flask could generate 355 ppm formaldehyde with 21% O_2/He balance gas, which was named as initial gas. The RH of initial gas was 45%. We investigated this reaction under different RH (RH = 0%, 25%, 45%, 75% and 90%). The RH adjusted by combination of two gases. One gas is the initial gas flow the drying tube generated gas with RH = 0%, the other gas is the 21% O_2/He balance gas flow into ultrapure water and then flow the boat shape flask containing formaldehyde solution. The gas flow rate was maintained at 40 mL·min^{-1}. The catalyst bed temperature was maintained at 25 °C, and the products were analyzed using a gas chromatograph equipped with a TCD detector. The conversion of HCHO was calculated based on the yield of CO_2. The equation of CO_2 yield is listed as follow.

$$CO_2\,\text{yield}(\%) = \frac{\text{The amount of } CO_2\,(\text{ppm})}{\text{The amount of initial HCHO}\,(\text{ppm})} \times 100$$

2.3.2. CO oxidation

The catalytic oxidation reactions were performed in a fixed bed reactor loaded with 0.2 g of catalyst (40–60 mesh). The reaction feed consisted of 200 ppm CO with the gas mixture (O_2: 21%, He: balance).

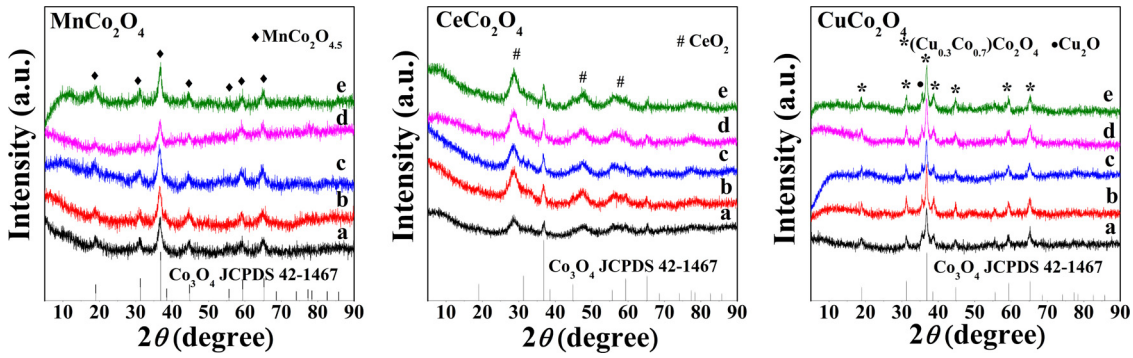

Fig. 1. XRD patterns of the fresh MCo_2O_4 (M = Mn, Ce, Cu) catalysts (a), used for HCHO oxidation in dry air (b) and in humid air (c), and used for CO oxidation in dry air (d) and in humid air (e), respectively. The RH of dry air is 0%. The RH of humid air is 45% for formaldehyde oxidation and 55% for CO oxidation, respectively.

The combined gas flow rate was maintained at 40 mL·min^{-1}. The humid condition was achieved with the reaction gas flow into the ultrapure water (RH = 0%, 25%, 45%, 75% and 90%). The catalyst bed temperature was maintained at 25 °C, and the reactants and products were analyzed using a gas chromatograph equipped with a TCD detector. The conversion of CO was calculated based on the yield of CO_2. The equation of CO_2 yield is listed as follow.

$$CO_2\,\text{yield}(\%) = \frac{\text{The amount of } CO_2\,(\text{ppm})}{\text{The amount of initial CO}\,(\text{ppm})} \times 100$$

3. Results and discussion

3.1. Characterization of MCo_2O_4 catalysts

The BET surface areas of Co_3O_4, $MnCo_2O_4$, $CeCo_2O_4$ and $CuCo_2O_4$ are 60.3, 123.8, 80.8 and 28.9 m^2·g^{-1}, respectively. The BET surface areas of $MnCo_2O_4$ and $CeCo_2O_4$ are larger than that of Co_3O_4, but the BET surface areas of $CuCo_2O_4$ is smaller than that of Co_3O_4. Fig. 1 showed the XRD patterns of the fresh MCo_2O_4 (M = Mn, Cu, Ce) catalysts and the related MCo_2O_4 used in HCHO oxidation and CO oxidation, respectively. The Co_3O_4 phase (JCPDS No.42-1467) was detected in all samples. The sharp diffraction peaks of the Co_3O_4 demonstrated the presence of the crystalline Co_3O_4 with a spinel structure [29]. As for the $MnCo_2O_4$, the peak at 31.3°, 36.8°, 44.8° and 59.5° are Co_3O_4 (220), Co_3O_4 (311), Co_3O_4 (400) and Co_3O_4 (511), respectively, which overlap with $MnCo_2O_{4.5}$ (220), $MnCo_2O_{4.5}$ (311), $MnCo_2O_{4.5}$ (400) and $MnCo_2O_{4.5}$ (511) (JCDPDS No. 32-0297), respectively. Thus, it can be concluded that the $MnCo_2O_4$ may be composed of both Co_3O_4 and $MnCo_2O_{4.5}$ phases, which was further confirmed by HRTEM results. In the case of $CeCo_2O_4$, the peaks at 28.5° and 47.5° are attributed to CeO_2 (111) and CeO_2 (220) (JCPDS No. 34-0394), respectively. For $CuCo_2O_4$, the peak at 36.5° is assigned to Cu_2O (111) (JCPDS No.75-1531) and the peaks at 19.0°, 31.3° and 38.6° are attributed to $(Cu_{0.3}Co_{0.7})Co_2O_4$ (111), $(Cu_{0.3}Co_{0.7})Co_2O_4$ (220) and $(Cu_{0.3}Co_{0.7})Co_2O_4$ (511), respectively. It is obvious that the diffraction peaks of the MCo_2O_4 catalysts used in HCHO and CO oxidation did not change compared with fresh MCo_2O_4.

The clear fringes observed in the HRTEM images (*Figure S1*) and the corresponding selected area electron diffraction (SAED) patterns (Figure S1 inset) indicate the high crystallinity of MCo_2O_4 (M = Mn, Ce and Cu). The SAED patterns of all the catalysts (fresh and used) indicate the polycrystalline structure of MCo_2O_4. For $MnCo_2O_4$, the bright diffraction rings can be indexed to the (220), (311), (400), and (511) crystal planes of Co_3O_4, which overlapped with (220), (311), and (400) of $MnCo_2O_{4.5}$, respectively. There is a bright diffraction ring that was assigned to Co_3O_4 (531). Therefore, $MnCo_2O_4$ is consistent with the cubic spinel structure of Co_3O_4 and $MnCo_2O_{4.5}$, which is in accordance with the XRD results. For $CeCo_2O_4$, there is a bright diffraction ring assigned to CeO_2 (111), and another bright diffraction ring assigned to Co_3O_4. For the $CuCo_2O_4$ samples, all bright diffraction rings could be assigned to $(Cu_{0.3}Co_{0.7})Co_2O_4$. In addition, the morphology and crystalline structure of the catalysts did not change after use in HCHO and CO reactions. XPS results indicate that the solid-state redox couples Co^{3+}/Co^{2+} and Mn^{4+}/Mn^{3+} coexist in $MnCo_2O_4$ catalyst. Co^{3+}/Co^{2+} and Ce^{4+}/Ce^{3+} coexist in $CeCo_2O_4$ catalyst. Co^{3+}/Co^{2+} and Cu^{2+}/Cu^{+} coexist in $CuCo_2O_4$ catalyst (*Figure S2*). The replacement of Co by other metal atoms will generate oxygen vacancies and may have good catalytic performance in oxidation reactions [19,20,30,31]. The Co atoms in Co_3O_4 replaced by Mn^{3+} or Ce^{3+} made $MnCo_2O_4$ and $CeCo_2O_4$ have more oxygen vacancies compared with Co_3O_4. The Co atoms in Co_3O_4 replaced by Cu^{+} could make $CuCo_2O_4$ have more oxygen vacancies. However, Cu_2O species were found in the synthesized $CuCo_2O_4$ sample (XRD results), which indicated that a certain of Cu^{+} were not used to generated oxygen vacancies. Thus, $CuCo_2O_4$ may have less oxygen vacancies compared with $MnCo_2O_4$ and $CeCo_2O_4$.

3.2. The oxygen vacancies investigation

The textural property of the Co_3O_4 and MCo_2O_4 catalysts was investigated by Raman spectroscopy (Fig. 2). The spectra of the fresh Co_3O_4 catalyst showed six Raman bands in the range of 100–850 cm^{-1}. The peak at 194, 478, 517 and 611 cm^{-1} were assigned to $F_{2g}^{(1)}$, E_g, $F_{2g}^{(2)}$, and $F_{2g}^{(3)}$ vibrational modes of Co_3O_4 spinel structure. The peak centered at 679 cm^{-1} was associated with A_{1g} symmetry of the Co_3O_4 phase. [32,33], The $MnCo_2O_4$ phase is identified from three broad peaks situated at 175, 478 and 600 cm^{-1}, which is correspond to $F_{2g}^{(1)}$, (E_g, $F_{2g}^{(2)}$), and ($F_{2g}^{(3)}$, A_{1g}) modes of the $MnCo_2O_4$, respectively [34]. The A_{1g} vibration of Co_3O_4 shift to lower frequency and has an increase in the width at half maximum of this band, which was attributed to a highly defective structure of the spinel structure [32,33]. Compared with 679 cm^{-1} peak of Co_3O_4 Raman spectra, a significant shift in the A_{1g} symmetry of $MnCo_2O_4$ toward lower frequency (600 cm^{-1}) accompanied with an increase in width at half maximum of this peak indicates that there are more defective sites in the Mn-rich $MnCo_2O_4$. The shift in the A_{1g} symmetry of $CeCo_2O_4$ at 650 cm^{-1} also indicates there are defective sites in $CeCo_2O_4$. However, compared with Co_3O_4 the peak associated with A_{1g} symmetry of $CuCo_2O_4$ toward higher frequency and without an increase in width at half maximum of this peak. Thus, there are no obvious defective sites in $CuCo_2O_4$ according to the Raman results.

As showed in Fig. 3A, the reduction behavior of Co_3O_4 and $MnCo_2O_4$ was investigated by TPR. The peaks at 340 and 440 °C in Co_3O_4 are attributed to the reduction of Co^{3+} to Co^{2+} and the reduction of Co^{2+} to Co, respectively [29]. For $MnCo_2O_4$ and $CeCo_2O_4$ catalysts, the peak attributed to the reduction of Co^{3+} to Co^{2+} shifts to 319 and 301 °C, respectively, indicated that an easier reduction of Co^{3+} to Co^{2+}. The peak at 245 and 512 °C in $MnCo_2O_4$ are assigned to

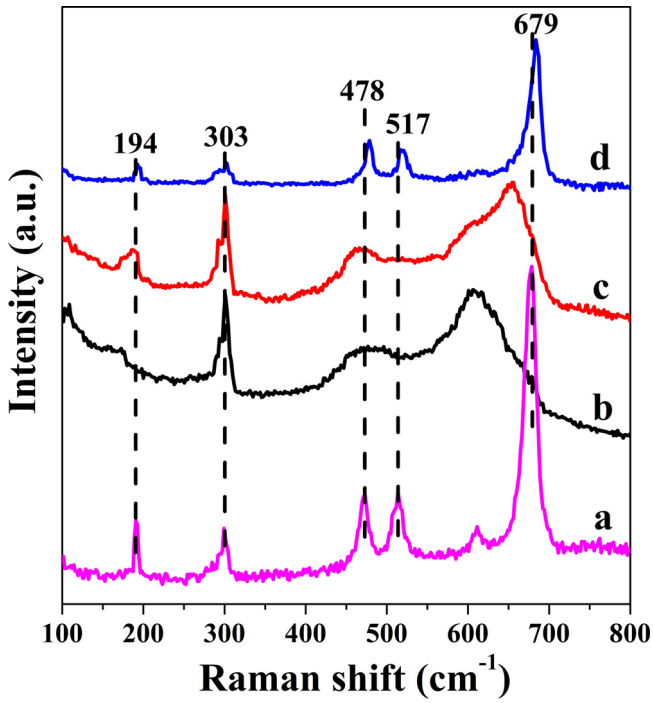

Fig. 2. Raman spectra of the fresh Co_3O_4 (a), $MnCo_2O_4$ (b), $CeCo_2O_4$ (c), $CuCo_2O_4$ (d) catalysts.

consumption of surface adsorbed oxygen and the reduction of Mn^{3+}, respectively [35]. The peak at 524 °C in $CeCo_2O_4$ is attributed to the reduction of Ce^{4+} [36]. The peak at 160 °C in $CuCo_2O_4$ is assigned to the reduction of Cu_2O. The intensity of the peak at 313 °C in $CuCo_2O_4$ is strong, which is attributed to both the reduction of Cu^{2+} to Cu^{+} and the reduction of Co^{3+} to Co^{2+} [29,37]. Compared with Co_3O_4, the reduction of Co^{3+} to Co^{2+} in all the MCo_2O_4 is easier. There is surface adsorbed oxygen in $MnCo_2O_4$ catalyst. The TPR results indicated that MCo_2O_4 catalysts have more surface oxygen and easy to reduction.

The adsorbed oxygen species on Co_3O_4 and MCo_2O_4 surface were investigated by O_2-TPD (Fig. 3B). Generally speaking, the desorption peaks of O_2^- and O^- located at less than 250 °C and the range of 300–700 °C, respectively. The O_2^- and O^- species are belonged to the surface active oxygen, which adsorbed on the oxygen vacancies. The desorption peaks located at more than 700 °C is ascribed to the bulk lattice oxygen [38]. The intensity of the peaks attributed to surface active oxygen followed this order: $MnCo_2O_4 > CeCo_2O_4 > CuCo_2O_4 \approx Co_3O_4$. Thus, compared with Co_3O_4, there are more oxygen vacancies in $MnCo_2O_4$ and $CeCo_2O_4$, and the oxygen vacancies in $CuCo_2O_4$ do not increase obviously.

3.3. The effect of H_2O on catalyst activity and stability

Fig. 4 showed the catalytic performance of HCHO and CO oxidation with time-on-stream over Co_3O_4 and MCo_2O_4 catalysts at 25 °C under different RH. Co_3O_4 does not show any catalytic activity for HCHO or CO oxidation. The RH of dry air is 0%. In dry air, $MnCo_2O_4$ gave the best catalytic activity and stability of HCHO oxidation. It was better than the activity and stability of $CeCo_2O_4$ and $CuCo_2O_4$ catalysts. In dry air, there is no HCHO conversion over $CuCo_2O_4$ catalysts due to less oxygen vacancies in $CuCo_2O_4$. The conversion of HCHO over $CeCo_2O_4$ steadily increased in the first 40 min and then decreased quickly. The $CeCo_2O_4$ was deactivated over 80 min in the HCHO oxidation reaction. In humid air (RH = 75%), the initial HCHO conversion over $CuCo_2O_4$ is 37%, and the $CuCo_2O_4$ also showed 12% HCHO conversion after 100 min. In humid air, the $CuCo_2O_4$ showed the activity of HCHO oxidation due to the promoted effect of H_2O on HCHO oxidation over $CuCo_2O_4$. When the RH increased to 90%, the HCHO conversion over $CuCo_2O_4$ decreased compared with RH = 75%. It may be attributed to modest amounts of H_2O are needed, but excess H_2O could covered a little part of the active sites. The HCHO conversion over $MnCo_2O_4$ and $CeCo_2O_4$ catalysts decreased more quickly in humid air than in dry air. Those results highlight the important role of H_2O in MCo_2O_4 catalysts for HCHO oxidation. The H_2O in reaction air promotes HCHO conversion over $CuCo_2O_4$ but prevents HCHO conversion over $MnCo_2O_4$ and $CeCo_2O_4$ catalysts. Zhang et al. [2] found that the activity of HCHO oxidation over the MnO_x catalyst increased at a certain initial humidity (RH = 33% and RH = 65%), but the catalytic activity decreased when the RH increased to 92%. The hydroxyl radical from water vapor dissociation was recognized to promote HCHO oxidation, which could not explain the activity decrease in humid air with RH = 92%. The effect of H_2O on catalyst activity and stability for HCHO oxidation was studied further by H_2O-TPD and DRIFT in this paper.

In dry air, the CO conversion over $MnCo_2O_4$ is higher than that over $CuCo_2O_4$ and $CeCo_2O_4$ catalysts. The CO conversion increased with time-on-stream over $MnCo_2O_4$ and reached 87%, and the CO conversion was maintained through 150 min. The initial CO_2 yields on $CeCo_2O_4$ and $CuCo_2O_4$ catalysts were 53.3% and 74.8%, respectively. The CO conversion over $CeCo_2O_4$ and $CuCo_2O_4$ declined until it was stable after approximately 125 min and 160 min, respectively. The CO conversions over $CeCo_2O_4$ and $CuCo_2O_4$ were 25% and 24% when the CO conversion over the catalysts was stable, respectively. Most importantly, the carbon monoxide conversion and carbon dioxide yields are about equal. In humid air (RH = 55%), the CO conversion over $MnCo_2O_4$ and $CuCo_2O_4$ catalysts declined sharply and had the same

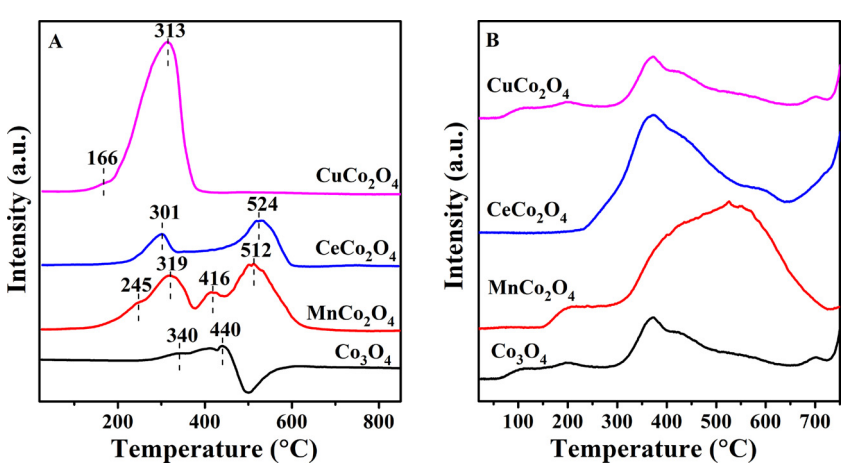

Fig. 3. H_2-TPR (A) and O_2-TPD (B) profiles of the fresh Co_3O_4 and MCo_2O_4 (M = Mn, Ce, Cu) catalysts.

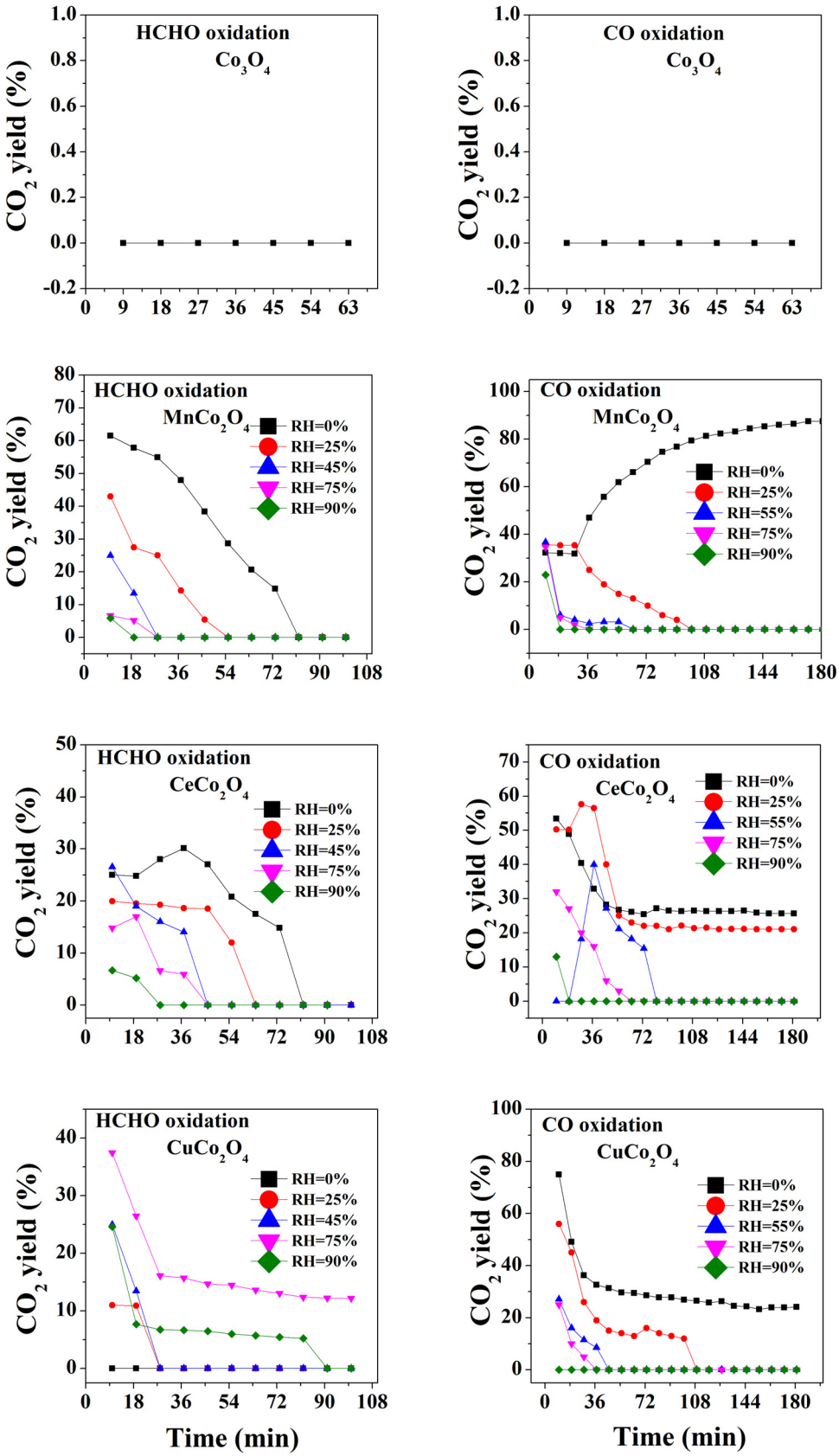

Fig. 4. Reaction tests at 25 °C for HCHO oxidation (A, C, E and G) and CO oxidation (B, D, F, H) with time-on-stream over Co_3O_4 and MCo_2O_4 (M = Mn, Ce, Cu) catalysts under different RH.

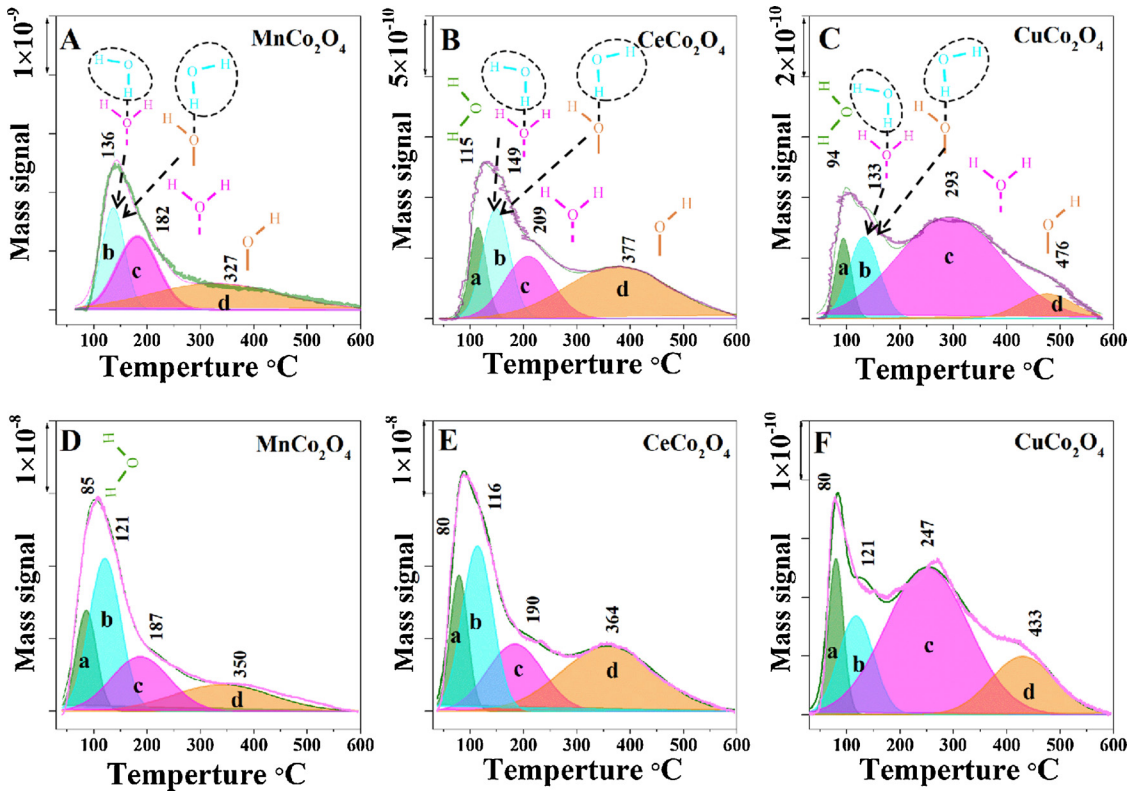

Fig. 5. H_2O-TPD profiles of the fresh MCo_2O_4 (M = Mn, Ce, Cu) catalysts and the deactivated MCo_2O_4 catalysts in HCHO oxidation in RH = 45% condition.

declining trend as HCHO conversion. The CO conversion over $CeCo_2O_4$ increased in the first 30 min and then decreased quickly until it was deactivated completely. In humid air (RH = 25%), the initial CO conversion over $CeCo_2O_4$ is 50%, and there is still 21% CO conversion after 180 min. CeO_2 shows good catalytic performance in water gas shift reaction. There is CeO_2 phase in $CeCo_2O_4$ catalyst. It is possible that in RH = 25% the H_2O has an interaction effect with CO over CeO_2 similar to a water gas shift process. All the MCo_2O_4 catalysts were deactivated for CO oxidation in humid air in 100 min except for $CeCo_2O_4$ in RH = 25% condition, but all the MCo_2O_4 catalysts showed CO conversion in dry air even at 180 min. It was indicated that H_2O in the reaction air induced deactivation of the MCo_2O_4 catalysts for CO oxidation.

3.4. The surface H_2O adsorption species on MCo_2O_4 catalysts

H_2O-TPD measurements were used to characterize the water-MCo_2O_4 interaction. Profiles of the normalized mass response of water *versus* the temperature of the fresh and the deactivated MCo_2O_4 catalysts are plotted in Fig. 5. The deactivated MCo_2O_4 catalysts were the MCo_2O_4 deactivated in formaldehyde oxidation under humid air (RH = 45%). In order to understand the water adsorption on the MCo_2O_4 catalysts, the profiles were fitted by a Gaussian-Lorentz function. The H_2O-TPD spectra of fresh $MnCo_2O_4$ contain three deconvoluted peaks at 136, 182 and 327 °C. The H_2O-TPD spectra of fresh $CeCo_2O_4$ contain four deconvoluted peaks at 115, 149, 209 and 377 °C. The H_2O-TPD spectra of fresh $CuCo_2O_4$ contain four deconvoluted peaks at 94, 133, 293 and 476 °C. The peak below 120 °C is attributed to H_2O included in the interparticle space and has no interaction with the MCo_2O_4 surface, which is defined as *type a* H_2O [39,40]. It can be seen that no H_2O was included in the interparticle space in the $MnCo_2O_4$ catalyst. The peak centered on the temperature between 120 and 150 °C is due to the H_2O interacting with surface-adsorbed water or hydroxide through hydrogen bonding (*type b* H_2O). The peak centered on the temperature between 150 and 300 °C is due to the H_2O associatively adsorbed on MCo_2O_4 catalysts (*type c* H_2O). The peak centered at the temperature above 300 °C is attributed to dehydration of structural hydroxides (*type d* H_2O). It has been reported that water vapor and surface active oxygen (O_2^-, $O^- + H_2O \rightarrow 2-OH$) can generate surface hydroxyl groups [40]. The terminal OH groups are ascribed to surface adsorbed oxygen species, which were thought to react with HCHO species [2]. Because the associatively adsorbed H_2O (*type c* H_2O) can provide active protons, the associatively adsorbed H_2O may be the active site for the oxidation reaction [40,41]. The other three type of H_2O are either hydrogen-bonded H_2O or dissociatively adsorbed H_2O without apparent activity. Although the percent of *type c* adsorption H_2O in fresh $CuCo_2O_4$ is higher compared with $MnCo_2O_4$ and $CeCo_2O_4$, the absolute value of *type c* H_2O in fresh $CuCo_2O_4$ is lower. The percent of *type c* adsorption H_2O in deactivated MCo_2O_4 catalysts is lower than that in fresh MCo_2O_4 catalysts (Table 1). Based on the above analysis, the hydroxyl groups of the associatively adsorbed H_2O may be the active oxygen species. Active oxygen is always generated on the oxygen vacancy on the catalyst surface [40,42,43]. Therefore, we can attribute the hydroxyl groups of the associatively adsorbed H_2O located on the oxygen vacancy to be the active sites, which can be reacted with HCHO

Table 1
The percent of different type of adsorbed H_2O on MCo_2O_4 catalysts caculated according to area of the fitted peaks in H_2O-TPD profiles.

Catalysts	*type a*[&] (%)	*type b*[&] (%)	*type c*[&] (%)	*type d*[&] (%)
$MnCo_2O_4$[#]	0	26.6	34.2	39.2
$MnCo_2O_4$[*]	16.0	38.0	20.6	29.3
$CeCo_2O_4$[#]	13.9	21.5	35.3	8.4
$CeCo_2O_4$[*]	11.8	23.2	22.8	25.4
$CuCo_2O_4$[#]	8.0	15.8	67.8	42.2
$CuCo_2O_4$[*]	10.8	15.8	56.2	17.2

[#] Fresh MCo_2O_4 catalysts.
[*] Deactivated MCo_2O_4 catalysts for formaldehyde oxidation in humid air.
[&] The type of surface H_2O adsorption species on MCo_2O_4 catalysts.

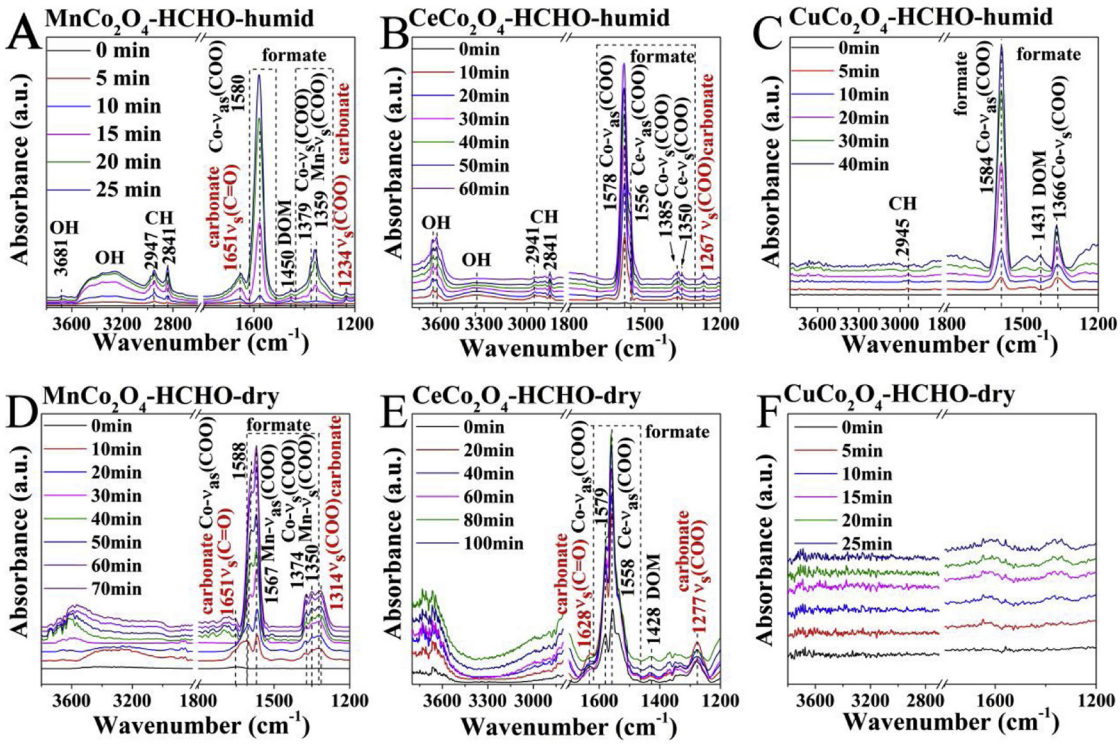

Fig. 6. *In-situ* DRIFTS spectra of HCHO oxidation in humid air (A, B and C) and in dry air (D, E and F) over MCo_2O_4 (M = Mn, Ce and Cu) catalysts. The RH of dry air is 0%. The RH of humid air is 45%.

species.

3.5. DRIFT study of the effect of H_2O on HCHO or CO oxidation

As shown in Fig. 6, *in situ* DRIFTS spectra of MCo_2O_4 (M = Mn, Ce, Cu) catalysts were obtained upon their exposure to dry HCHO reaction gas (RH = 0%) or humid HCHO reaction gas (RH = 45%). Both bands at 1567 and 1588 cm^{-1} are attributed to the asymmetric stretch ν_{as} (COO) of formate. The band at 1567 cm^{-1} is due to ν_{as} (COO) of formate adsorbed on Mn sites [2]. The band at 1588 cm^{-1} is due to ν_{as} (COO) of formate adsorbed on the other metal sites (Co sites). The bands at 1350 and 1374 cm^{-1} are due to the symmetric stretch ν_s (COO) of formate species adsorbed on Mn sites and Co sites, respectively [2,17]. The bands located in the range from 2700 to 3000 cm^{-1} can be ascribed to the stretching mode ν (CH) of formate species [2,44,45]. The bands at 1234, 1314, and 1651 cm^{-1} are assigned to asymmetric stretch ν_{as} (COO), symmetric stretch ν_s (COO) and symmetric stretch ν_s (C=O) of carbonate species, respectively [2]. The band at 1450 cm^{-1} is attributed to the bending mode δ (CH_2) of dioxymethylene (DOM) species, which is found on the $MnCo_2O_4$ and $CuCo_2O_4$ catalysts exposed in humid HCHO reaction gas and $CeCo_2O_4$ catalyst exposed in dry HCHO reaction gas. The DOM contains C–O bonds, but formate species contain C=O bonds. There is no carbonate species detectable on $CuCo_2O_4$ catalysts exposed to humid HCHO reaction gas. The ν_{as} (COO) and ν_s (COO) of formate only adsorbed on the Co site of the $CuCo_2O_4$ catalyst. However, the ν_{as} (COO) and ν_s (COO) of formate adsorbed on the Mn and Co sites of $MnCo_2O_4$ and the Ce and Co sites of the $CeCo_2O_4$ catalyst. Actually, when the formate species were oxidized further and transformed into CO_2, the complete oxidation of HCHO was achieved, and the formate species are the intermediates. However, if the formate species could not be transformed into CO_2, the formate species adsorbed on the active sites resulted in catalyst deactivation. The $MnCo_2O_4$ and $CeCo_2O_4$ catalysts deactivated in humid air more quickly than which in dry air. As shown in Fig. 6A and B, a broad band at 3200-3500 cm^{-1} and a narrow peak at 3681 cm^{-1} were attributed to hydrogen-bonded OH groups and free OH groups, respectively [40]. It can be seen that the intensity of hydrogen-bonded OH and free OH increased with time-on-stream for $MnCo_2O_4$ catalysts used in humid air. Based on the H_2O-TPD result analysis, $MnCo_2O_4$ catalyst tended to react with H_2O to generate different adsorbed H_2O and OH species. The associatively adsorbed H_2O (*type c* H_2O) may be the active site for the oxidation reaction, which can provide active protons. In humid air, if H_2O molecule adsorbed on the active *type c* H_2O, then the active *type c* H_2O will turned into inactive *type b* H_2O. The intensity of hydrogen-bonded OH increased as shown in DRIFT results (Fig. 6A), which stand for inactive *type b* H_2O generated on active *type c* H_2O sites. That $MnCo_2O_4$ catalyst being deactivated in humid air more quickly is attributed to both formate and hydrogen-bonded OH species that covered the active sites, but in dry air, only formate species adsorbed on active sites. The peak of free OH is strong for the $CeCo_2O_4$ catalyst used in humid air. This free OH is saturated with surface hydroxyl groups, which are stable and difficult to desorb from the catalyst surface [40]. The adsorbed formate species on $CeCo_2O_4$ active sites and free OH covering active sites also explain $CeCo_2O_4$ deactivation in humid air.

Fig. 7 showed that *in situ* DRIFTS spectra of CO oxidation over MCo_2O_4 (M = Mn, Ce, Cu) catalysts in dry air (RH = 0%) or in humid air (RH = 55%). For CO oxidation over $MnCo_2O_4$ catalyst in humid air, symmetric stretch ν_s(C=O) of carbonate species were detected. Carbonate species are intermediate for CO oxidation over $MnCo_2O_4$ catalyst in humid air. For CO oxidation over MCo_2O_4 (M = Ce or Cu) catalysts in humid air and CO oxidation over MCo_2O_4 (M = Mn or Ce) catalysts in dry air, we can observe the ν_{as} (COO) of formate and symmetric stretch ν_s (C=O) of carbonate. So both the formate and carbonate were identified as intermediate. First, CO was oxidized to formate, and formate was oxidized to carbonate further. The carbonate decomposed into CO_2 and H_2O. The ν_{as} (COO) and ν_s (COO) of formate were observed for CO oxidation over $CuCo_2O_4$ catalyst in dry air. The formate species are intermediate for CO oxidation over $CuCo_2O_4$ catalyst in dry air.

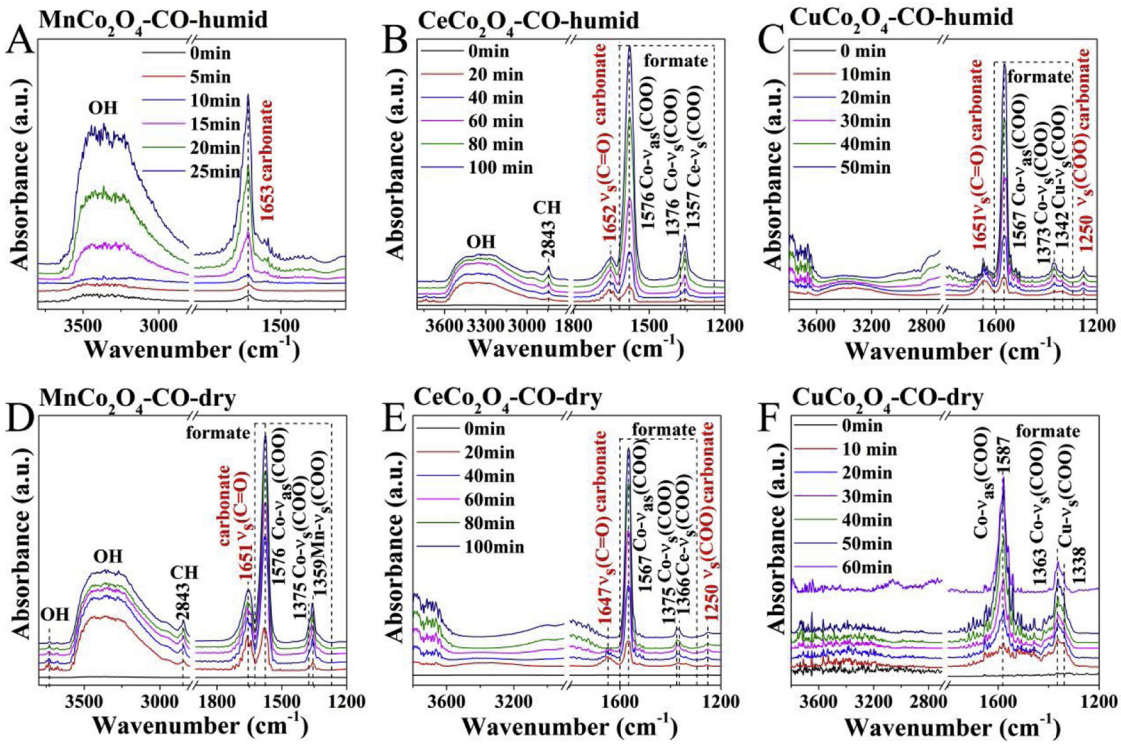

Fig. 7. *In-situ* DRIFTS spectra of CO oxidation in humid air (A, B and C) and in dry air (D, E and F) over MCo_2O_4 (M = Mn, Ce and Cu) catalysts. The RH of dry air is 0%. The RH of humid air is 55%.

3.6. Mechanism of the effect of H_2O on HCHO and CO oxidation

The MCo_2O_4 oxides showed increased catalytic activities in the oxidation reactions due to the enhanced formation of oxygen vacancies [19,20]. The addition of Mn, Ce or Cu enhanced the oxygen vacancies of Co_3O_4 oxide. The active oxygen species generated on the oxygen vacancies of the catalysts run the oxidation reactions, which is the reason that MCo_2O_4 oxides have shown catalytic activities of HCHO and CO oxidation but Co_3O_4 oxide showed no catalytic activities. The reaction and deactivation mechanism of HCHO oxidation over MCo_2O_4 at room temperature is shown in Fig. 8. First, the associatively adsorbed H_2O on the oxygen vacancies provided active HOH sites, and the O atom of HCHO is adsorbed on the H atom of HOH sites. It has been reported that the surface OH facilitates the oxidation of HCHO [2,16,19,22,46]. Here, we confirm the surface OH come from active HOH sites, because HOH sites are unstable and can provide active protons. The HOH active species generated on the $CuCo_2O_4$ catalyst are more difficult than in $MnCo_2O_4$ and $CeCo_2O_4$ catalysts (as shown in Fig. 5). Thus, only in humid air can the $CuCo_2O_4$ convert HCHO to CO_2 because H_2O vapor contributes to the HOH generated on the $CuCo_2O_4$ catalyst. Second, the C=O bond of the adsorbed HCHO broke and formed an intermediate that included a carbon atom bonded to two oxygen atoms (−COO), which is called a formate group. The electron environment of the two oxygen atoms is different, and the formate group is not stable, which will be transformed into carbonate or CO_2. With time, the formate group will accumulate and turn to be stable, which cannot be transformed into CO_2. The HOH active sites were covered by formate groups, which led to catalyst deactivation. Ji et al. [47] found that the formate oxidation is the rating determining step in formaldehyde oxidation promoted by active oxygen and hydroxyl together. Hydrogen-bonded OH species adsorbed on active HOH sites resulted in that $MnCo_2O_4$ catalyst deactivated more quickly in humid air than in dry air. The $CeCo_2O_4$ catalyst deactivated more quickly in humid air than in dry air, which is attributed to free OH species adsorbed on active HOH sites.

It has been reported that surface OH groups are inactive for CO oxidation at low temperature [10,19,25]. Thus, the first step for CO oxidation is the CO adsorbed on the MCo_2O_4 (M = Mn, Ce, Cu) catalysts. Then, O_2 molecule is activated on the oxygen vacancy of catalyst to form active oxygen species (O_2^- and O^-). The adsorbed CO reacted with active oxygen species (not include OH species) to form intermediates, such as formate or carbonate. Finally, the intermediates were oxidized into CO_2 and H_2O. In humid air, H_2O adsorbed on the oxygen vacancies will block O_2 activation on the oxygen vacancies, which induced the deactivation of MCo_2O_4 catalysts for CO oxidation.

4. Conclusions

We synthesized MCo_2O_4 (M = Mn, Ce, Cu) catalysts and investigated the effect of H_2O on the catalytic activity and stability of HCHO and CO oxidation over MCo_2O_4 catalysts. The $MnCo_2O_4$ and $CeCo_2O_4$ catalysts deactivated more quickly for HCHO oxidation in humid air than in dry air. $CuCo_2O_4$ showed initial activity of HCHO oxidation in humid air. In dry air (RH = 0%), $CuCo_2O_4$ is inactive for HCHO oxidation. For $CuCo_2O_4$, the H_2O is beneficial for the generation of associatively adsorbed H_2O, which acts as an active oxygen species in HCHO oxidation. In the existence of H_2O, the hydrogen-bonded OH generated on $MnCo_2O_4$ and free OH generated on $CeCo_2O_4$ will cover the active sites and speed catalyst deactivation in HCHO oxidation. In both HCHO and CO oxidation, formate species are found to be an intermediate, which are further oxidized into carbonate or directly to CO_2. The other reason of MCo_2O_4 catalysts deactivation in HCHO oxidation is that the formate species adsorbed on the active sites becomes stable and cannot be transformed to CO_2. The associatively adsorbed H_2O is not the active oxygen species for CO oxidation. The reason of MCo_2O_4 catalysts deactivation in CO oxidation in humid air is that H_2O molecule adsorbed on oxygen vacancies and blocked the generation of active oxygen species.

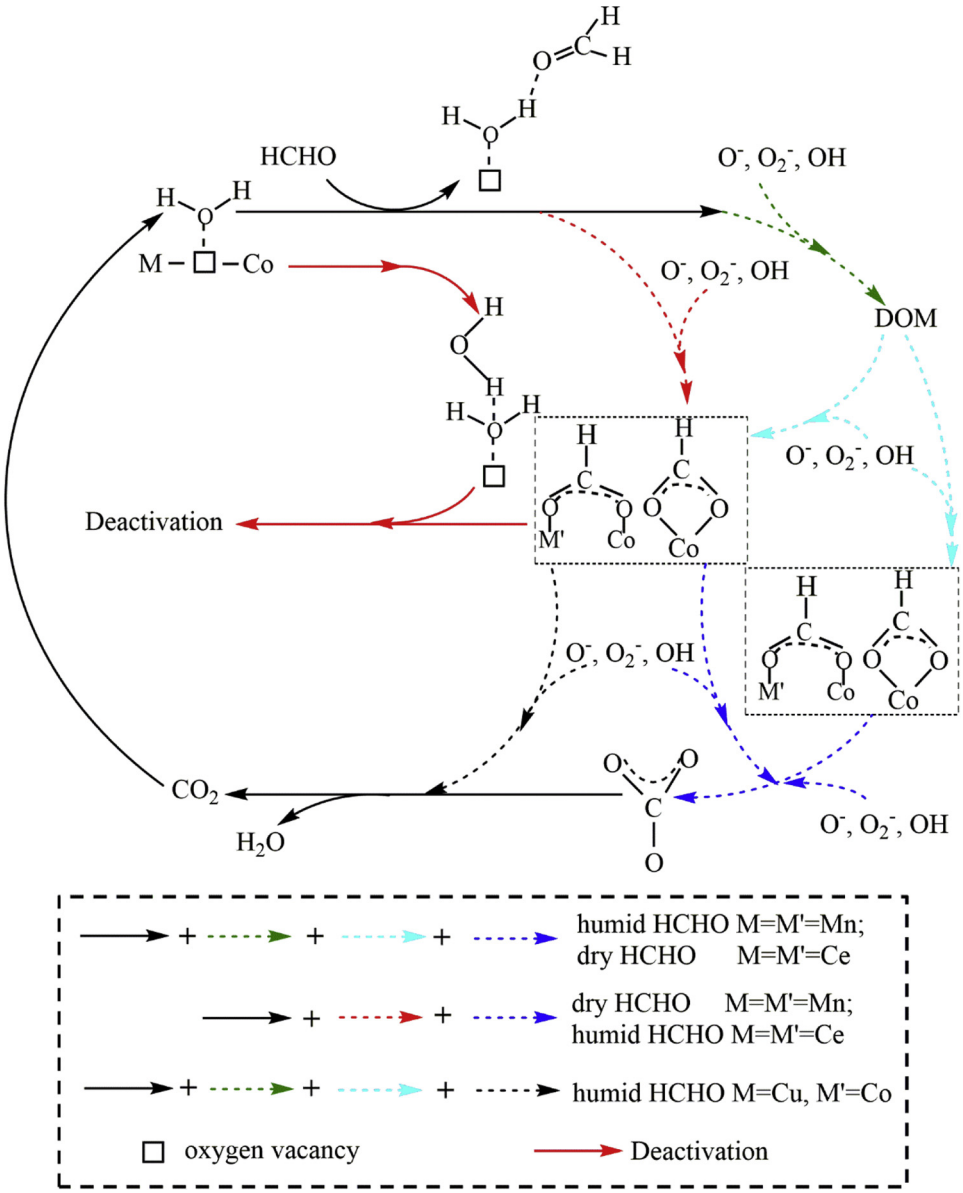

Fig. 8. Proposed mechanism of HCHO oxidation at room temperature over MCo_2O_4 (M = Mn, Ce and Cu) catalysts.

Acknowledgements

This work was supported by the National Natural Science Foundation of China (21777175 and 21477148), and Key Research Program of Frontier Sciences, CAS (QYZDB-SSW-DQC018). We thank Dr. Xiaole Weng (Zhejiang University) for the H_2O-TPD measurement.

Appendix A. Supplementary data

Supplementary material related to this article can be found, in the online version, at doi:https://doi.org/10.1016/j.apcatb.2019.04.085.

References

[1] J.P. Pinto, G.R. Gladstone, Y.L. Yung, Photochemical production of formaldehyde in earth's primitive atmosphere, Science 210 (1980) 183–185, https://doi.org/10.1126/science.210.4466.183.

[2] J. Wang, P. Zhang, J. Li, C. Jiang, R. Yunus, J. Kim, Room-temperature oxidation of formaldehyde by layered manganese oxide: effect of water, Environ. Sci. Technol. 49 (2015) 12372–12379, https://doi.org/10.1021/acs.est.5b02085.

[3] C. Ma, X. Li, T. Zhu, Removal of low-concentration formaldehyde in air by adsorption on activated carbon modified by hexamethylene diamine, Carbon 49 (2011) 2873–2875, https://doi.org/10.1016/j.carbon.2011.02.058.

[4] J.L. Shie, C.H. Lee, C.S. Chiou, C.T. Chang, C.C. Chang, C.Y. Chang, Photodegradation kinetics of formaldehyde using light sources of UVA, UVC and UVLED in the presence of composed silver titanium oxide photocatalyst, J. Hazard. Mater. 155 (2008) 164–172, https://doi.org/10.1016/j.jhazmat.2007.11.043.

[5] T. Noguchi, A. Fujishima, P. Sawunyama, K. Hashimoto, Photocatalytic degradation of gaseous formaldehyde using TiO_2 film, Environ. Sci. Technol. 32 (1998) 3831–3833, https://doi.org/10.1021/es980299+.

[6] M.B. Chang, C.C. Lee, Destruction of formaldehyde with dielectric barrier discharge plasmas, Environ. Sci. Technol. 29 (1995) 181–186, https://doi.org/10.1021/es00001a023.

[7] J. Wang, J. Li, P. Zhang, G. Zhang, Understanding the "seesaw effect" of interlayered K^+ with different structure in manganese oxides for the enhanced formaldehyde oxidation, Appl. Catal. B: Environ. 224 (2018) 863–870, https://doi.org/10.1016/j.apcatb.2017.11.019.

[8] L. Yu, R. Peng, L. Chen, M. Fu, J. Wu, D. Ye, Ag supported on CeO_2 with different morphologies for the catalytic oxidation of HCHO, Chem. Eng. J. 334 (2018) 2480–2487, https://doi.org/10.1016/j.cej.2017.11.121.

[9] J. Zhang, Y. Li, L. Wang, C. Zhang, H. He, Catalytic oxidation of formaldehyde over manganese oxides with different crystal structures, Catal. Sci. Technol. 5 (2015) 2305–2313, https://doi.org/10.1039/c4cy01461h.

[10] L. Minh Thang, N. The Tien, P. Phuong Thi Mai, E. Bruneel, I. Van Driessche, Activated MnO_2-Co_3O_4-CeO_2 catalysts for the treatment of CO at room temperature, Appl. Catal. A Gen. 480 (2014) 34–41, https://doi.org/10.1016/j.apcata.2014.04.034.

[11] C.B. Zhang, H. He, K. Tanaka, Catalytic performance and mechanism of a Pt/TiO_2

catalyst for the oxidation of formaldehyde at room temperature, Appl. Catal. B: Environ. 65 (2006) 37–43, https://doi.org/10.1016/j.apcatb.2005.12.010.
[12] D. Chen, Z. Qu, Y. Sun, K. Gao, Y. Wang, Identification of reaction intermediates and mechanism responsible for highly active HCHO oxidation on Ag/MCM-41 catalysts, Appl. Catal. B: Environ. 142–143 (2013) 838–848, https://doi.org/10.1016/j.apcatb.2013.06.025.
[13] M. Daté, M. Okumura, S. Tsubota, M. Haruta, Vital role of moisture in the catalytic activity of supported gold nanoparticles, Angew. Chem. Int. Ed. 43 (2004) 2129–2132, https://doi.org/10.1002/anie.200453796.
[14] A.S.K. Hashmi, G.J. Hutchings, Gold catalysis, Angew. Chem. Int. Ed. 45 (2006) 7896–7936, https://doi.org/10.1002/anie.200602454.
[15] C. Zhang, F. Liu, Y. Zhai, H. Ariga, N. Yi, Y. Liu, K. Asakura, M. Flytzani-Stephanopoulos, H. He, Alkali-metal-promoted Pt/TiO_2 opens a more efficient pathway to formaldehyde oxidation at ambient temperatures, Angew. Chem. Int. Ed. 51 (2012) 9628–9632, https://doi.org/10.1002/anie.201202034.
[16] J. Quiroz, J.M. Giraudon, A. Gervasini, C. Dujardin, C. Lancelot, M. Trentesaux, J.F. Lamonier, Total oxidation of formaldehyde over MnO_x-CeO_2 catalysts: the effect of acid treatment, ACS Catal. 5 (2015) 2260–2269, https://doi.org/10.1021/cs501879j.
[17] C. Ma, D. Wang, W. Xue, B. Dou, H. Wang, Z. Hao, Investigation of formaldehyde oxidation over Co_3O_4-CeO_2 and Au/Co_3O_4-CeO_2 catalysts at room temperature: effective removal and determination of reaction mechanism, Environ. Sci. Technol. 45 (2011) 3628–3634, https://doi.org/10.1021/es104146v.
[18] Y. Sekine, Oxidative decomposition of formaldehyde by metal oxides at room temperature, Atmos. Environ. 36 (2002) 5543–5547, https://doi.org/10.1016/S1352-2310(02)00670-2.
[19] Y. Wang, X. Zhu, M. Crocker, B. Chen, C. Shi, A comparative study of the catalytic oxidation of HCHO and CO over $Mn_{0.75}Co_{2.25}O_4$ catalyst: the effect of moisture, Appl. Catal. B: Environ. 160–161 (2014) 542–551, https://doi.org/10.1016/j.apcatb.2014.06.011.
[20] C. Shi, Y. Wang, A. Zhu, B. Chen, C. Au, $Mn_xCo_{3-x}O_4$ solid solution as high-efficient catalysts for low-temperature oxidation of formaldehyde, Catal. Commun. 28 (2012) 18–22, https://doi.org/10.1016/j.catcom.2012.08.003.
[21] X. Xie, Y. Li, Z.-Q. Liu, M. Haruta, W. Shen, Low-temperature oxidation of CO catalysed by Co_3O_4 nanorods, Nature 458 (2009) 746–749, https://doi.org/10.1038/nature07877.
[22] X. Tang, Y. Li, X. Huang, Y. Xu, H. Zhu, J. Wang, W. Shen, MnO_x-CeO_2 mixed oxide catalysts for complete oxidation of formaldehyde: effect of preparation method and calcination temperature, Appl. Catal. B: Environ. 62 (2006) 265–273, https://doi.org/10.1016/j.apcatb.2005.08.004.
[23] J. Jansson, Low-temperature CO oxidation over Co_3O_4/Al_2O_3, J. Catal. 194 (2000) 55–60, https://doi.org/10.1006/jcat.2000.2924.
[24] Y. Yu, T. Takei, H. Ohashi, H. He, X. Zhang, M. Haruta, Pretreatments of Co_3O_4 at moderate temperature for CO oxidation at -80°C, J. Catal. 267 (2009) 121–128, https://doi.org/10.1016/j.jcat.2009.08.003.
[25] F. Grillo, M.M. Natile, A. Glisenti, Low temperature oxidation of carbon monoxide: the influence of water and oxygen on the reactivity of a Co_3O_4 powder surface, Appl. Catal. B: Environ. 48 (2004) 267–274, https://doi.org/10.1016/j.apcatb.2003.11.003.
[26] H. Zou, X. Dong, W. Lin, Selective CO oxidation in hydrogen-rich gas over CuO/CeO_2 catalysts, Appl. Surf. Sci. 253 (2006) 2893–2898, https://doi.org/10.1016/j.apsusc.2006.06.028.
[27] K. Sirichaiprasert, A. Luengnaruemitchai, S. Pongstabodee, Selective oxidation of CO to CO_2 over Cu-Ce-Fe-O composite-oxide catalyst in hydrogen feed stream, Int. J. Hydrogen Energy 32 (2007) 915–926, https://doi.org/10.1016/j.ijhydene.2006.10.060.
[28] G. Marbán, A.B. Fuertes, Highly active and selective CuO_x/CeO_2 catalyst prepared by a single-step citrate method for preferential oxidation of carbon monoxide, Appl. Catal. B: Environ. 57 (2005) 43–53, https://doi.org/10.1016/j.apcatb.2004.10.011.
[29] B. Bai, H. Arandiyan, J. Li, Comparison of the performance for oxidation of formaldehyde on nano-Co_3O_4, 2D-Co_3O_4, and 3D-Co_3O_4 catalysts, Appl. Catal. B: Environ. 142 (2013) 677–683, https://doi.org/10.1016/j.apcatb.2013.05.056.
[30] X. Weng, P. Sun, Y. Long, Q. Meng, Z. Wu, Catalytic oxidation of chlorobenzene over $Mn_xCe_{1-x}O_2$/HZSM-5 catalysts: a study with practical implications, Environ. Sci. Technol. 51 (2017) 8057–8066, https://doi.org/10.1021/acs.est.6b06585.
[31] W.H. Bragg, The structure of magnetite and the spinels, Nature 95 (1915) 561, https://doi.org/10.1038/095561a0.
[32] Q. Ren, Z. Feng, S. Mo, C. Huang, S. Li, W. Zhang, L. Chen, M. Fu, J. Wu, D. Ye, 1D-Co_3O_4, 2D-Co_3O_4, 3D-Co_3O_4 for catalytic oxidation of toluene, Catal. Today (2018), https://doi.org/10.1016/j.cattod.2018.06.053.
[33] B. Xiao, K. Zhao, L. Zhang, T. Cai, X. Zhang, Z. Wang, J. Yuan, L. Yang, P. Gao, D. He, A green and facile synthesis of Co_3O_4 monolithic catalyst with enhanced total oxidation of propane performance, Catal. Commun. 116 (2018) 1–4, https://doi.org/10.1016/j.catcom.2018.07.013.
[34] A. Gaur, M.A. Mohiddon, V.M. Sglavo, Phenomenological understanding of flash sintering in $MnCo_2O_4$, J. Eur. Ceram. Soc. 38 (2018) 4543–4552, https://doi.org/10.1016/j.jeurceramsoc.2018.06.006.
[35] L. Zhu, J. Wang, S. Rong, H. Wang, P. Zhang, Cerium modified birnessite-type MnO_2 for gaseous formaldehyde oxidation at low temperature, Appl. Catal. B: Environ. 211 (2017) 212–221, https://doi.org/10.1016/j.apcatb.2017.04.025.
[36] J. Mei, J. Xie, Y. Sun, Z. Qu, N. Yan, Design of Co_3O_4/CeO_2-Co_3O_4 hierarchical binary oxides for the catalytic oxidation of dibromomethane, J. Ind. Eng. Chem. 73 (2019) 134–141, https://doi.org/10.1016/j.jiec.2019.01.016.
[37] Y. Yi, C. Li, L. Zhao, X. Du, L. Gao, J. Chen, Y. Zhai, G. Zeng, The synthetic evaluation of CuO-MnO_x-modified pinecone biochar for simultaneous removal formaldehyde and elemental mercury from simulated flue gas, Environ. Sci. Pollut. Res. 25 (2018) 4761–4775, https://doi.org/10.1007/s11356-017-0855-8.
[38] Z. Wang, W. Wang, L. Zhang, D. Jiang, Surface oxygen vacancies on Co_3O_4 mediated catalytic formaldehyde oxidation at room temperature, Catal. Sci. Technol. 6 (2016) 3845–3853, https://doi.org/10.1039/C5CY01709B.
[39] A. Setiawan, E.M. Kennedy, B.Z. Dlugogorski, A.A. Adesina, M. Stockenhuber, The stability of Co_3O_4, Fe_2O_3, Au/Co_3O_4 and Au/Fe_2O_3 catalysts in the catalytic combustion of lean methane mixtures in the presence of water, Catal. Today 258 (2015) 276–283, https://doi.org/10.1016/j.cattod.2014.11.031.
[40] Y. Wang, F. Wang, Q. Song, Q. Xin, S. Xu, J. Xu, Heterogeneous ceria catalyst with water-tolerant Lewis acidic sites for one-pot synthesis of 1,3-diols via Prins condensation and hydrolysis reactions, J. Am. Chem. Soc. 135 (2013) 1506–1515, https://doi.org/10.1021/ja310498c.
[41] H. Yang, C. Ma, X. Zhang, Y. Li, J. Cheng, Z. Hao, Understanding the active sites of Ag/zeolites and deactivation mechanism of ethylene catalytic oxidation at room temperature, ACS Catal. 8 (2018) 1248–1258, https://doi.org/10.1021/acscatal.7b02410.
[42] B. Qiu, M. Zhang, L. Wu, J. Wang, Y. Xia, D. Qian, H. Liu, S. Hy, Y. Chen, K. An, Y. Zhu, Z. Liu, Y.S. Meng, Gas-solid interfacial modification of oxygen activity in layered oxide cathodes for lithium-ion batteries, Nat.Commun. 7 (2016) 12108, https://doi.org/10.1038/ncomms12108.
[43] D.N. Pei, L. Gong, A.Y. Zhang, X. Zhang, J.J. Chen, Y. Mu, H.Q. Yu, Defective titanium dioxide single crystals exposed by high-energy {001} facets for efficient oxygen reduction, Nat. Commun. 6 (2015) 8696, https://doi.org/10.1038/ncomms9696.
[44] C. Li, K. Domen, K.I. Maruya, T. Onishi, Spectroscopic identification of adsorbed species derived from adsorption and decomposition of formic acid, methanol, and formaldehyde on cerium oxide, J. Catal. 125 (1990) 445–455, https://doi.org/10.1016/0021-9517(90)90317-D.
[45] J.S. Chung, C.O. Bennett, On the shift in the CH stretching bands of methoxy groups chemisorbed on metal oxides, J. Catal. 92 (1985) 173–176, https://doi.org/10.1016/0021-9517(85)90247-7.
[46] T. Yang, Y. Huo, Y. Liu, Z. Rui, H. Ji, Efficient formaldehyde oxidation over nickel hydroxide promoted Pt/γ-Al_2O_3 with a low Pt content, Appl. Catal. B: Environ. 200 (2017) 543–551, https://doi.org/10.1016/j.apcatb.2016.07.041.
[47] X. Wang, Z. Rui, H. Ji, DFT study of formaldehyde oxidation on silver cluster by active oxygen and hydroxyl groups: mechanism comparison and synergistic effect, Catal. Today (2018), https://doi.org/10.1016/j.cattod.2018.06.021.